Chandra HRC-S Degapping Corrections

Vinay L. Kashyap, Jeremy J. Drake, and Sun Mi Chung

CXC/SAO, 60 Garden St., MS-83, Cambridge, MA, USA

ABSTRACT

The HRC-S is a microchannel plate detector on board *Chandra* and is primarily used for spectroscopic observations with the Low Energy Transmission Grating Spectrometer (LETGS) in place. Photons are detected via signals read out from evenly spaced wires underneath the plates and positions are computed by centroiding around the strongest amplifier signals. This process leads to gaps in between the taps where no events are placed. A deterministic correction is then made during ground processing to these event locations to remove the gaps. We have now developed a new, empirical degap corrections from flight data. We describe the procedure we use, present comparisons between the new degap and lab-data based degap, and investigate the temporal stability of the degap corrections.

Keywords: *Chandra*, HRC-S, LETG, degapping, dispersion, continuum sources

1. INTRODUCTION

The *Chandra* X-ray Observatory[1] is a high-resolution imaging telescope in an eccentric, deep-space orbit. One of the instruments on board is the High Resolution Camera (HRC; a set of multi-channel plate detectors, MCPs)[2] that use a crossed grid charge detector[3] to register the locations of X-ray events to a precision of $\approx 6.43\,\mu$m, or $0.132''$. The HRC has an intrinsic spectral resolution of $\frac{\Delta E}{E} \approx 1$ at 1 keV, but when used in conjunction with the Low Energy Transmission Grating Spectrometer (LETGS), a resolution of 0.05 Å FWHM, corresponding to a spread over ≈ 8 pixels, can be achieved. The performance of the LETGS is strongly tied to the accuracy of the position determination of the photons. Here we consider the effects of a primary characteristic of the HRC position determination algorithm that directly affects its accuracy and consequently the wavelength registration of grating data.

The LETGS is primarily used in conjunction with the spectroscopic array, the HRC-S.[4] The HRC-S consists of 3 MCPs, with 1513 wires along the dispersion direction (the V-axis) and 121 wires along the cross-dispersion direction (the U-axis) with a wire pitch of 0.2057 mm. An amplifier taps into this crossed grid at every eighth wire, with the result that there are 190 and 16 "taps" along the V and U axes respectively. The charge cloud generated by an incoming photon at the base of the MCP is read out by these amplifiers, and the position of the event is determined using the so-called "three-tap algorithm".[3] The tap with the strongest signal is designated as the site of the event, and the position is further refined by combining the signal from this amplifier, say A_i, with those from the adjacent taps to determine the fine position

$$f_p = \frac{A_{i+1} - A_{i-1}}{A_{i+1} + A_i + A_{i+1}} \,. \tag{1}$$

However, because charge in taps beyond the nearest ones is uncollected, this results in gaps near the edge of the taps where there will be a deficit of events (see top left plots of Figure 1). Note that unlike telescope vignetting, pileup, or Quantum Efficiency (QE), this is not lossy (i.e., the photons are not lost; they are simply mispositioned) and can be deterministically corrected with a suitably constructed degapping algorithm.[5]

The degapping algorithm currently used for *Chandra* data analysis (the "CALDB degap") was derived by fitting symmetric 5th-order polynomials around tap center, to lab data.[6] This algorithm still has some defects, such as a 1-pixel drop-off between taps, invalid corrections due to the assumed symmetry of the degapping, etc. These errors have been suspected to be the cause of the observed non-linearities in the LETGS+HRC-S dispersion relation.[7] Here we seek to verify the CALDB degap using on-orbit data, and update the degapping

coefficients for V taps to assist in the LETGS wavelength calibration. We have developed a new approach to the problem that relies on making empirical corrections. We list the datasets used for this analysis in §2, and briefly describe the data reduction, extraction, and the derivation of the empirical degapping parameters in §3. The results are described in §4 and summarized in §5.

2. DATA

We have chosen a number of continuum sources which were observed with the HRC-S+LETG to determine the degapping parameters along the dispersion axis of the instrument. The datasets chosen (see Table 1) include both sources that were observed expressly for calibration purposes (e.g., PKS 2155-304, HZ 43, Sirius B) as well as GO (e.g., Mkn 421, RXJ 1856) and DDT observations (RXJ 1856), and cover the entire timeline of *Chandra*'s operation from 1999 till 2003. This last factor allows us to explore the time dependency of degapping corrections. We coadd data from PKS 2155-304, HZ 43, Mkn 421, and Sirius B in our derivation of degapping parameters.

Table 1. Observation ID numbers of datasets used

Source	1999	2000	2001	2002	2003
PKS 2155-304	331	1704	1013,3166	3709	...
HZ 43	59,1170	...	1011,1012	2584,2585	3676
Mkn 421	...	...	...	...	4149
RXJ 1856.5-3754	...	113	3380,3381,3382	...	...
Sirius B	1421,1452,1459	...	...	...	...

3. ANALYSIS

The HRC-S poses some unique practical difficulties in the determination of degapping solutions using on-orbit data. Due to an uncorrectable error in the onboard electronics, the anticoincidence counter has been turned ineffective, and the telemetered data contain a large number of particle events, which strongly affects the pattern of the amplifier signals, and adversely affects the degapping solution. These background events are reduced, but never entirely eliminated, using various filtering steps during analysis. Therefore, degapping solutions are strongly tied to the filtering applied to the data.[*] Further, the analysis naturally depends on photons dispersed by the LETGS, whose numbers depend on the shape of the source spectrum and the telescope effective area, and hence there are less data available on the outer plates. Note that it is imperative that the true distribution of the photons across a tap be known exactly, or else the degap solution will be subject to large systematic errors. Hence we limit our analysis to continuum sources, which minimize large deviations within a tap.

3.1. Reduction and Extraction

In all cases, we begin with the so-called Level 1 event files, which lists the amplifier signals in three adjacent taps for each event, along each axis. The fine positions are computed as in Eqn. 1, including other corrections such as the tap-ringing correction[5] and the amplifier scale corrections.[9]

The pipeline derived SKY coordinates are then used to filter the data to extract events along the dispersion axis. The dispersion axis is determined using previously degapped and aspect-corrected data. Events falling within this region are included as source photons. This ensures that we extract the relevant photons in a narrow strip and thus minimize the contribution of the background events. The background events are further reduced by status-bit filtering which accounts for various instrument-based diagnostics, and by removing all events with $PI = 255$. We estimate that at the end of this process, the contribution of the background events is $\approx 10\%$.

[*]For instance, the CALDB degap is derived from data which has been filtered with the so-called H-test,[8] while flight data from HRC-S are not.

The remaining events are then binned into a spectrum, and then the aspect solution is used to undither it to the spectrum as it would be seen in detector coordinates. The raw event distributions in each tap are then required to match this spectral shape. This has the advantage that the gross shape of the photon distribution across the taps is properly accounted for, though small-scale irregularities in the QE are not. An example of the actual event distribution and the model are shown in the top left plots of Figure 1.
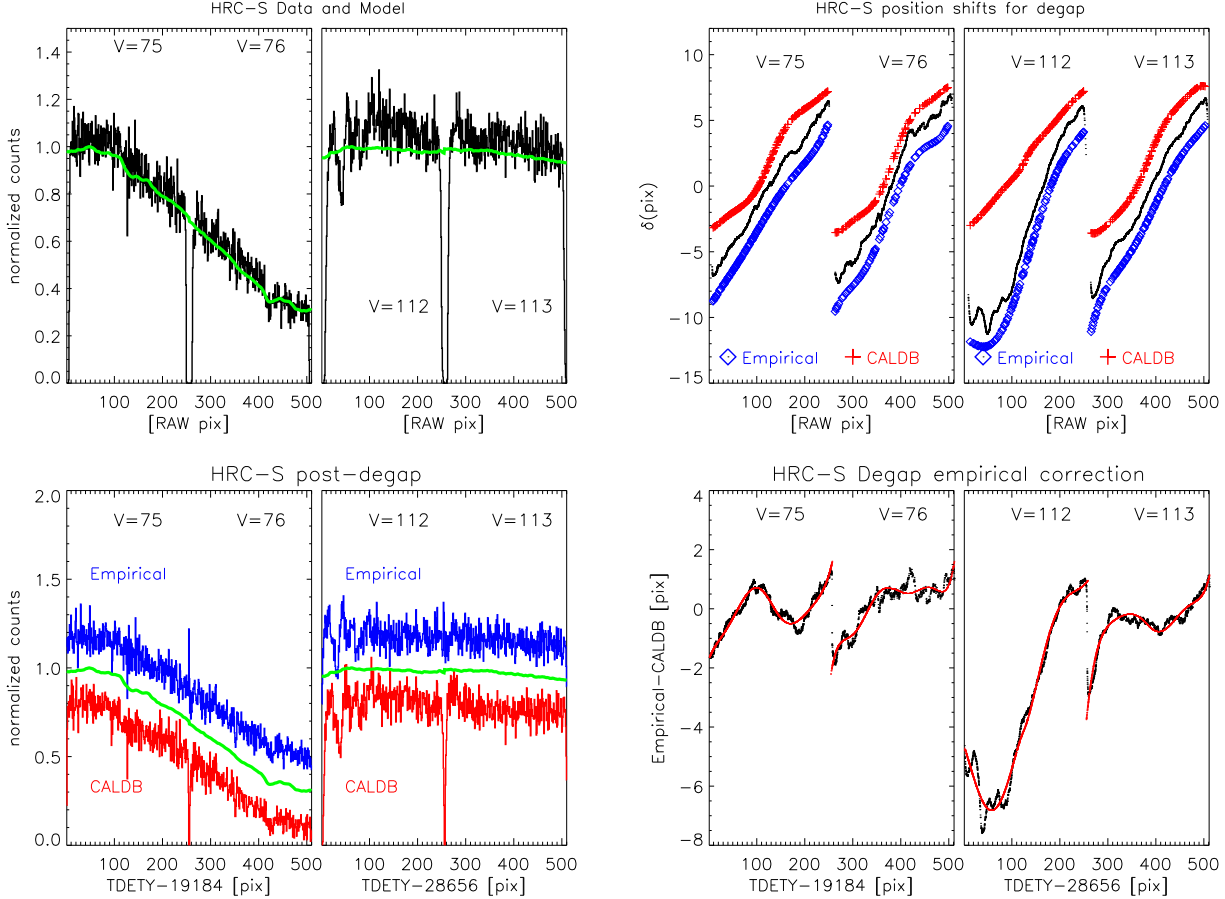

Figure 1. TOP LEFT: Raw counts distribution across a tap, illustrating the gap between taps. The light solid line is the expected distribution of the counts, based on the observed spectrum. Two sets of adjacent taps are shown: the set on the left spans the C edge along the +ve dispersion and shows the need for proper modeling of the spectrum; the set on the right is near ≈ -25Å, and is ostensibly better behaved, i.e., flatter, but note the scalloping at the left edge. **TOP RIGHT:** Position shifts required to fill out the gaps between taps. The empirically determined correction is shown as the thin line. Also shown, offset for clarity, are the current CALDB implementation of the degap correction (pluses; shifted upwards), and a 5th-order polynomial fit to the empirical solution (diamonds; shifted downwards). Note the large difference between the CALDB and empirical solutions for tap 112. **BOTTOM LEFT:** As in the plots at top left, but for degapped data in tiled detector coordinates. The data are shown for corrections made with different methods, and offset from the exact solution (thick light solid line) for clarity. The CALDB solution (shifted downwards) still shows a residual 1-pixel gap, which has been eliminated in the empirical polynomial solution (5th-order polynomial fit to the exact solution; shifted upwards). **BOTTOM RIGHT:** The correction to the CALDB degap. The difference between the position shifts derived from the CALDB degap and the empirical solution are shown for the same taps as above. The smooth line represents the differences between the CALDB degap and the $5th$-order polynomial fit to the empirical degap. Note that the empirical degap removes the scalloping at the left edge of tap 112, while the polynomial fit does not.

3.2. Degapping Procedure

If the expected distribution of the degapped data over a tap is flat, then the observed distribution of fine positions can be flattened (and consequently degapped) by sorting the events by current location, and then moving the ith event to the location $f_p^{emp} = \frac{i}{N} - 0.5$ relative to the center of the tap, where N is the total number of events. Such a transformation would result in a histogram of events that is exactly flat. Hence, the degapping correction would be

$$\delta_{pix} = f_p^{emp} - f_p \,. \tag{2}$$

That is, if photons at fine position f_p are moved by a distance δ_{pix}, the distribution of events across the tap will become identically flat. When the expected distribution is not flat, the degapping correction can be calculated in a space where the model shape has been transformed to be flat. This is equivalent to computing $f_p^{emp} = F(i) - 0.5$, where $F(i)$ is the cumulative representation of the model shape, such that $F(0) = 0$ and $F(N) = 1$.

Note that the exact solution as derived above is defined for the location of all the photons, and inherently includes the effects of statistical errors in the data. We summarize this solution by averaging the derived δ_{pix} over small (1-pixel) ranges of f_p. This is then used to correct the event locations in other observations that utilize the HRC-S (e.g., in studies of non-linearities in the dispersion relation[10]). We have also fit 5th-order polynomials to the exact solution in order to facilitate its incorporation into the *Chandra* calibration database in the future. An example of the degapping solution δ_{pix} is illustrated in the top right plots of Figure 1, as derived from the data shown at top left of the same figure. Applying the degap correction results in the events being redistributed across the tap with no gaps left in between (see bottom left plots of Figure 1). The empirical degap solution differs significantly from the CALDB solution (see bottom right plots of Figure 1).

3.3. Limitations

As alluded to above, the empirical degapping solution derived here is dependent on a number of factors. These include the filtering steps used to reduce the background, the selection of a suitable continuum source, and proper modeling of the counts distribution across a tap.

Note that background cannot be subtracted out, nor can the background events be perfectly identified and eliminated from the analysis. We have applied stringent filters to the data to reduce the amount of background contamination to on average $\approx 10\%$, to about 20 counts in each bin. The contamination is higher at the extreme ends of the detector where there are fewer source counts in general. Thus, the degap solutions are most reliable in the center chip. Efforts to improve the filtering and to decrease the background in other ways are ongoing.

Further, when the counts distribution model shape changes steeply (e.g., at the 0th-order, at plate gaps, or at detector edges), the degap solution may be subject to systematic errors whose magnitude depends on the accuracy of the modeling, i.e., the accuracy of the aspect solution. These systematic errors usually lead to large deviations in the degap solutions which can be easily identified. Also, the solutions do not take into account small-scale variations in QE across a tap which may be inadvertently smoothed out. In other words, the empirical degap solution is only as good as the model.

We also assume that the order of the events as a function of fine position remains unchanged after applying the degapping correction, and that all events are affected. While these are reasonable assumptions, their validity has not been established.

Finally, we have explored the temporal stability of the degap solutions (see §4.2 below), and find some significant changes in the required corrections over the years. Such changes must be better characterized, and incorporated, in the degap solution.

4. RESULTS

4.1. Empirical Degap

The empirical degapping correction to the CALDB degap is shown in Figure 2, which shows the corrections for all 3 MCPs. The values shown must be added to the pixel position shifts derived with the CALDB degap to obtain the correct degap shifts. Note the recurring pattern in the corrections, where taps corresponding to similar locations on the MCPs all show similar behavior (e.g., compare the regions around taps 48, 112, and 175
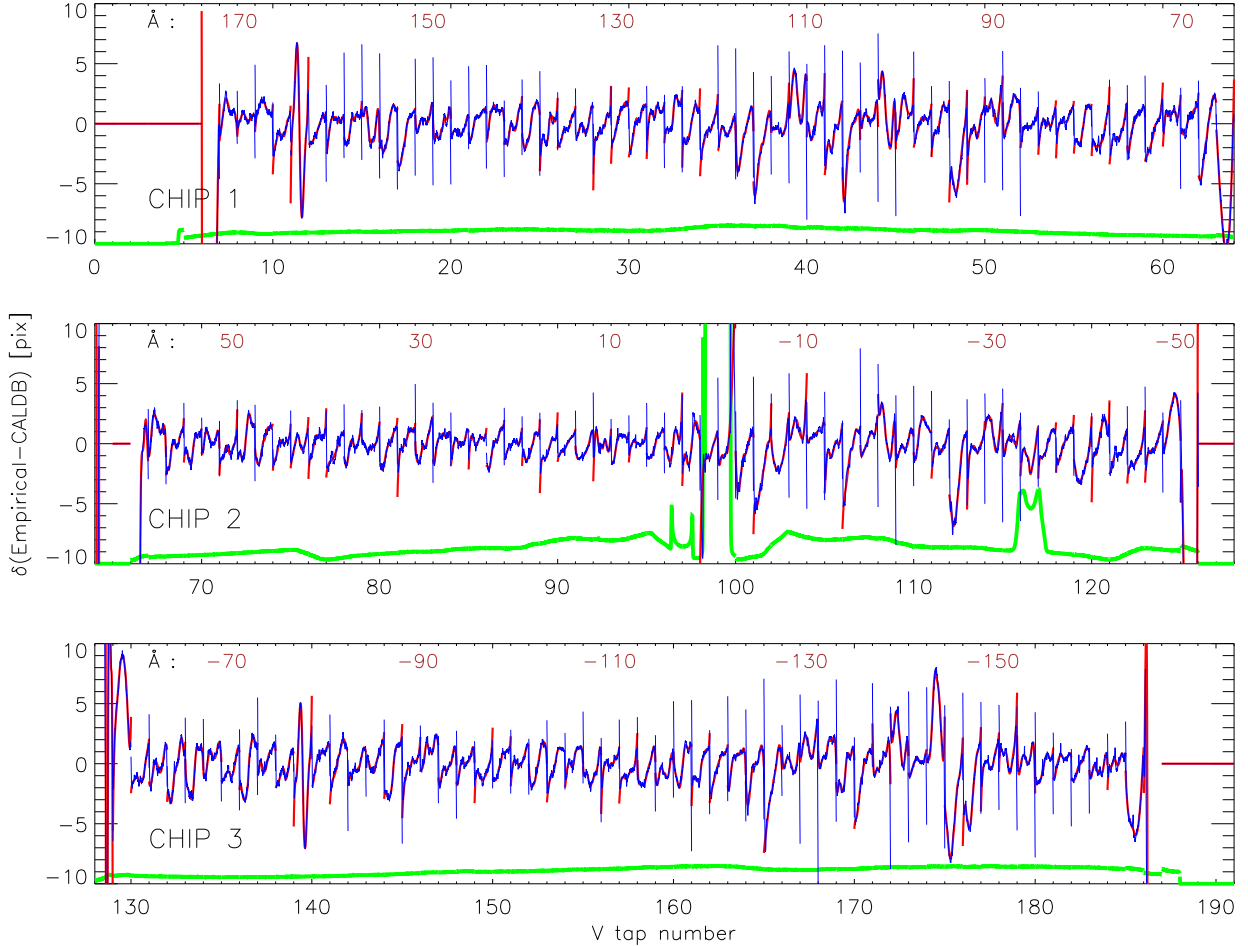
Figure 2. Empirical correction to the CALDB degapping solution for all taps along the dispersion axis, for HRC-S1 (top panel), HRC-S2 (middle panel), and HRC-S3 (bottom panel). The difference in pixel shifts between the empirical and CALDB solutions are plotted. A pixel covers $6.43\,\mu$m, or $0.0067\,$Å on the dispersion scale; for context, the line response function has a FWHM of $0.05\,$Å, or ~ 8 pixels. Also shown in the lower part of each panel is the spectrum used to determine the true distribution of counts over a tap (solid light line); this is offset and rescaled to arbitrary linear units for purposes of illustration. Note the large spikes corresponding to the locations of the zeroth orders of the coadded data. The approximate wavelength scale for a nominal pointing is shown along the top of each plot.

in Chips 1, 2, and 3 respectively). This behavior was previously identified in an analysis of tap amplifier signals of flight data,[11] and has now been confirmed with the empirical degap solution.

In order to summarize the magnitude of the correction for each tap, we consider the mean absolute differences between the CALDB and empirical degap solutions in Figure 3. Note the large errors at chip gaps and at the 0th-order locations; improved modeling for these regions is in progress. In general, the average correction is ~ 2 pix (the vertical bars), but in certain locations within the tap, the correction may be as large as $6-8$ pix.

The CALDB degap is calculated assuming that the corrections are symmetric around tap center, and that the correction at tap center is zero. Our measurements however show that both assumptions are invalid at almost all taps, with the zero-point (i.e., that position along the tap which requires no degapping correction at all) being many tens of pixels away from tap center. There is no discernible pattern to these shifts in the zero-point; changes in the zero-point towards both positive and negative f_p are seen (see Figure 3).

To demonstrate that the empirical degapping solution works, we have applied it to a line source, Capella.
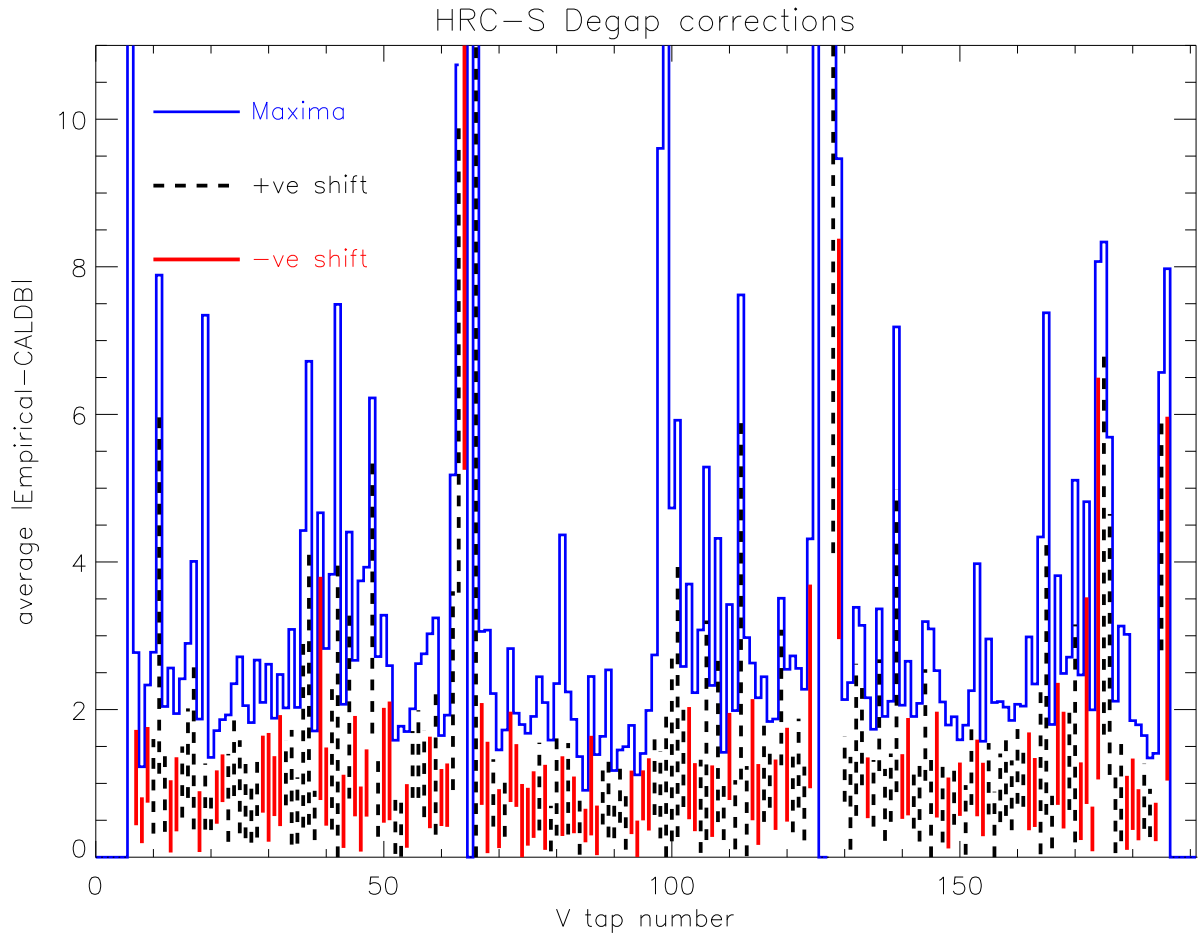
Figure 3. A tap-wise summary of the magnitude of the corrections. The maximum positional shift difference between the CALDB and the empirical degapping solutions are shown as the solid histogram, and estimates of the mean absolute differences are shown as vertical bars, the sizes of which represent the standard deviations in the absolute differences. The CALDB solution assumes that the degap correction at the middle of the tap is zero; the empirical solution does not make that assumption, and taps where the zero-point is shifted to the right are displayed with dashed vertical bars, and those where the zero-point is shifted to the left are displayed with solid vertical bars.
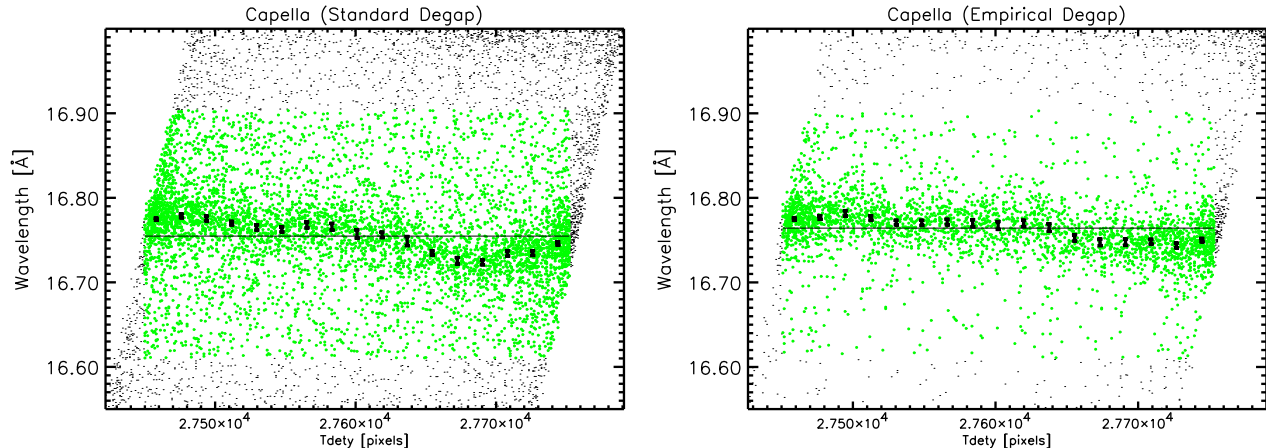
Figure 4. LETGS+HRC-S dispersion non-linearities as seen from the deviations in a spectral line from Capella. **Left:** Tiled detector positions along the dispersion axis (and corresponding wavelengths) with the CALDB degap applied. The horizontal line indicates the measured location of the Fe XVII line, and the black dots represent best-fit locations over small regions of TDETY, derived by binning the photons (shown as light dots) and fitting β-profiles to them. **Right:** Same as left panel, but using the empirically determined degap corrections. This correction clearly brings the events into line better than the CALDB degap, though there are some as yet unexplained residuals.

In Figure 4, we show the region of the spectrum corresponding to the Fe XVII line, with degapping corrections applied using the CALDB degap and the empirical degap. It is clear that the empirical degap aligns the photons better than the CALDB degap, though there are residual deviations that are still unexplained.

4.2. Temporal Variations

As pointed out in §2 and Table 1, we have sufficient temporal coverage with our chosen datasets to explore the possible time dependency of the degapping solution. That is, we can construct a degapping solution for each year of Chandra's operation and compare them with each other to determine whether they have remained stable. However, breaking the full coadded data into yearly groups means that the statistical error on the degap solutions increases for each group. The reduced number of counts also increases the propensity for systematic errors, since a Poisson fluctuation in one bin can be a significant fraction of the counts in that bin, and thereby causes nonlinear horizontal shifts in the run of δ_{pix}. We estimate the magnitude of these systematic errors by comparing observed counts in a bin to the statistical error in adjacent bins, and adopting their inverse ratio as an estimate of the magnitude of the systematic error.

The mean absolute yearly change in the degap correction is shown in Figure 5 as vertical bars. In order to estimate the significance of these quantities, we derive a variability index in the form of a χ^2 estimate by taking the square of the ratio of the yearly differences and the square-added errors. This index is shown in Figure 5 as a histogram for all of the taps. Taps where it exceeds 4 are unstable. In order to be conservative, we have chosen the maximum systematic error in each tap as being representative of the systematic error in that tap. We note that each chip has a few taps which show an yearly change that is inconsistent with expected statistical fluctuations. A thorough analysis of the error budget is still in progress and more taps may be flagged as unstable in the future.

5. SUMMARY

Using LETGS+HRC-S data, we have constructed new degapping corrections for the HRC-S detector for taps along the dispersion axis. We compute the position shifts to the raw positions that are necessary to remove the gaps between the taps and compare these to the degapping solution derived from lab data. We find significant differences between the two, consistent with recent independent findings of amplifier mismatches in the HRC-S
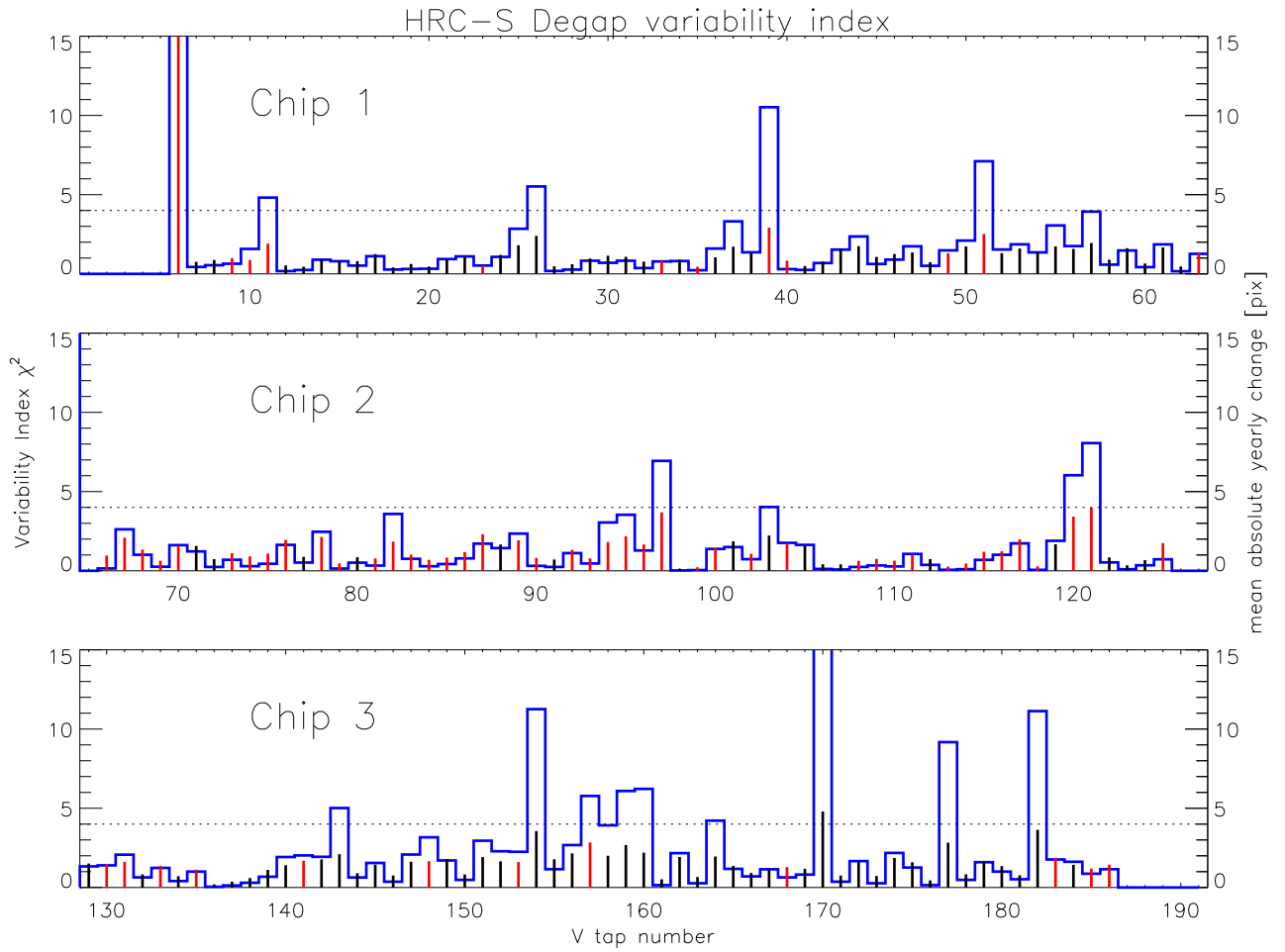
Figure 5. Temporal stability of the degapping solutions for the 3 chips (top: HRC-S1; middle: HRC-S2; bottom: HRC-S3). For each tap along the dispersion axis, χ^2-like index, the square of the ratio of the mean change per year to the error is calculated, and plotted as the solid histogram. The errors include both statistical and systematic components, the latter which are conservatively overestimated. Values of the variability index that lie above the dotted line indicate taps with unstable solutions. Also shown as vertical bars are the mean absolute yearly change in the degap positional correction for each tap (scale on right hand side).

and non-linearities in the LETGS dispersion relation. In general, the differences are of sufficient magnitude to account for the non-linearities in the dispersion relation, but in practice do not fully explain these non-linearities. We also estimate the temporal stability of the degap solution, and find that certain regions of the detector are prone to large changes over timescales of years.

ACKNOWLEDGMENTS

REFERENCES

1. `http://asc.harvard.edu/`
2. S. S. Murray, and J. H. Chappell, "The Advanced X-ray Astrophysics High Resolution Camera", Proc. SPIE, 982, 77, 1988
3. J. H. Chappell, and S. S. Murray, "Position Modeling for the AXAF High Resolution Camera (HRC)", Proc. SPIE, 1159, 460, 1989
4. A. Kenter, R. Goddard, J. Gomes, J. Lessing, S. S. Murray, R. Moore, R. Roll, M. Valenza, and M. V. Zombeck, "MCP Readout for the AXAF-I Grating Spectrometer", Proc. SPIE, 2009, 84, 1993
5. M. Juda, G. K. Austin, J. H. Chappell, J. J. Gomes, A. T. Kenter, R. P. Kraft, S. S. Murray, and M. V. Zombeck, "Improving Chandra High Resolution Camera event positions via corrections to crossed-grid charge detector signals", Proc. SPIE, 4140, 155, 2000
6. A. Kenter, "Present Degap Procedure for the HRC detectors", Proc. of the 2002 Chandra Calibration Workshop
7. S. M. Chung, J. J. Drake, V. L. Kashyap, P. W. Ratzlaff, and B. J. Wargelin, "Characterizing nonlinearities in the Chandra LETGS + HRC-S dispersion relation", Proc. SPIE, 5165, 518, 2004
8. S. S. Murray, J. H. Chappell, A. T. Kenter, M. Juda, R. P. Kraft, M. V. Zombeck, G. R. Meehan, G. K. Austin, and J. J. Gomez "Event screening for the Chandra X-Ray Observatory High-Resolution Camera (HRC)", Proc. SPIE, 4140, 144, 2000
9. M. Juda, "An Improved AMP_SF Correction Scheme",
   `http://cxc.harvard.edu/contrib/juda/memos/amp_scale/improved_scale_correction.html`
10. S. M. Chung, J. J. Drake, and V. L. Kashyap, "Non-Linearities of the Chandra LETG+HRC-S Dispersion Relation", SPIE, 5488-62, 2004
11. M. Juda, "Amplifier Mismatch as a Possible Source of HRC Event Position Distortions", Proc. of the 2003 Chandra Calibration Workshop
    `http://cxc.harvard.edu/ccw/proceedings/03_proc/presentations/juda/index.html`